Surface Chemistry of Quantum Dots Determines Their Behavior in Postischemic Tissue

Markus Rehberg,[†,*] Camila F. Leite,[†] Karina Mildner,[‡] Jan Horstkotte,[§] Dagmar Zeuschner,[‡] and Fritz Krombach[†]

[†]Walter Brendel Centre of Experimental Medicine, Ludwig-Maximilians-Universität München, Munich, Germany, [‡]MPI for Molecular Biomedicine, Münster, Germany, and [§]Medizinische Klinik I, Klinikum der Universität München, 81377 Munich, Germany

ABSTRACT

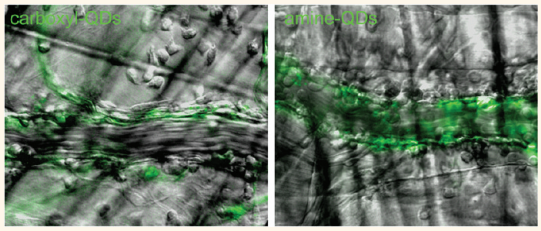

The behavior of quantum dots (QDs) in the microvasculature and their impact on inflammatory reactions under pathophysiological conditions are still largely unknown. Therefore, we designed this study to investigate the fate and effects of surface-modified QDs in postischemic skeletal and heart muscle. Under these pathophysiological conditions, amine-modified QDs, but not carboxyl-QDs, were strongly associated with the vessel wall of postcapillary venules and amplified ischemia-reperfusion-elicited leukocyte transmigration. Importantly, strong association of amine-QDs with microvessel walls was also present in the postischemic myocardium. As shown by electron microscopy and verified by FACS analyses, amine-modified QDs, but not carboxyl-QDs, were associated with endogenous microparticles. At microvessel walls, these aggregates were attached to endothelial cells. Taken together, we found that both the surface chemistry of QDs and the underlying tissue conditions (*i.e.*, ischemia-reperfusion) strongly determine their uptake by endothelial cells in microvessels, their association to endogenous microparticles, as well as their potential to modify inflammatory processes. Thus, this study strongly corroborates the view that the surface chemistry of nanomaterials and the physiological state of the tissue are crucial for the behavior of nanomaterials *in vivo*.

KEYWORDS: quantum dots · nanoparticles · surface modifications · inflammation · *in vivo* microscopy · microcirculation · ischemia-reperfusion

Over the last several years, the development and production of nanomaterials have been vastly expanding.[1] Different types of nanosized materials, including quantum dots (QDs), are tested for nanomedical applications,[2] for targeting of tumors and other tissues for drug delivery, diagnosis, and treatment.[3−6] QDs exhibit unique fluorescent properties that make them ideally suited for novel imaging approaches.[4] More recently, various nanomaterials were applied for imaging and therapeutic purposes in ischemic tissues.[7−11]

In most of these approaches, nanomaterials are directly injected into the systemic circulation. Beyond that, it is well-established that various nanosized materials can penetrate biobarriers (*i.e.*, lungs, skin, gut) and thus transfer into the bloodstream.[12−14] The vascular system, in particular, the microvasculature comprising the capillary network as well as pre- and postcapillary vessels, plays a fundamental role in numerous regulatory, metabolic, and immunologic functions. Therefore, a detailed knowledge of the interactions of nanoparticles with vessel walls, of their uptake from the bloodstream, and of their potential to cross the blood−tissue border is crucial for biomedical applications as well as to assess their potential impact on physiological or pathophysiological processes—more so since nanosized ambient particulate matter has been implicated in cardiovascular disorders including myocardial infarction[15] and ischemia-reperfusion injury.[16] Ischemia-reperfusion (I/R) injury is one of the main causes of organ dysfunction or failure after myocardial infarction, hemorrhagic shock, and transplantation. Reperfusion of ischemic tissues is often related with microvascular dysfunction, enhanced microvascular permeability, and extravasation of leukocytes in postcapillary venules.[17] On the one hand, it has been shown that the extent of postischemic tissue damage strongly correlates with the number of leukocytes recruited to the reperfused tissue.[18−20] On the other hand, extravasated leukocytes are suggested to play a role in tissue remodeling and healing.[21−23]

Leukocyte recruitment from the microvasculature to the extravascular compartments

* Address correspondence to markus.rehberg@lrz.uni-muenchen.de.

Received for review October 31, 2011 and accepted January 14, 2012.

Published online January 15, 2012
10.1021/nn204187c

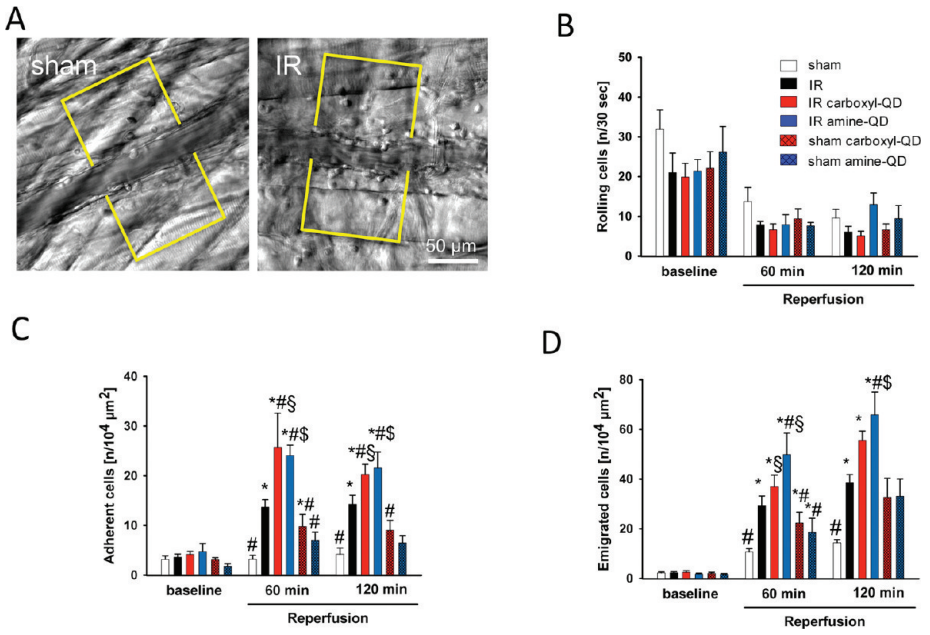

Figure 1. Effect of carboxyl- and amine-QDs on postischemic leukocyte responses. (A) Postcapillary venule in the postischemic cremaster tissue (I/R) surrounded by extravasated leukocytes. For comparison, a postcapillary venule of a sham-operated animal is shown (sham). Regions of interest for quantitative analysis of leukocyte recruitment parameters are indicated (yellow frames). Quantitative analysis of parameters of leukocyte–endothelial cell interactions and leukocyte emigration after QDs (3 pmol/g of BW) injection at the onset of reperfusion. Leukocyte rolling (B), firm adherence (C), and transmigration (D) in mice undergoing I/R (mean ± SEM; $n = 6$ per group; *$p < 0.05$ *vs* sham, #$p < 0.05$ *vs* IR, §$p < 0.05$ IR carboxyl-QDS *vs* sham carboxyl-QDs, $$p < 0.05$ IR amine-QDs *vs* sham amine-QDs).

is a tightly regulated multistep process. Endothelial adhesion molecules facilitate capture and rolling of leukocytes along the vessel wall. Rolling leukocytes are then activated by the interaction with chemokines presented or secreted by endothelial cells leading to arrest and firm adhesion of leukocytes mediated by leukocyte integrins and endothelial cell adhesion molecules. Subsequently, leukocytes emigrate through the vascular wall into the interstitial tissue.[24,25]

In two recent *in vivo* studies performed in healthy mice, we have investigated the fate and effects in the microvasculature of QDs of the same size but with different surface modifications.[26,27] We reported that the surface chemistry of QDs strongly affects their localization in postcapillary venules and their potential to modify steps of leukocyte recruitment.[27] Furthermore, we have demonstrated that the capillary endothelium considerably contributes to blood clearance and tissue deposition of anionic QDs.[26]

However, the interactions of QDs with microvessels and their impact on inflammatory reactions under pathophysiological conditions are still largely unknown. Therefore, we designed this study to investigate the impact of surface modification (i) on the microvascular localization of QDs and (ii) on the effects of QDs on the steps of leukocyte recruitment during ischemia-reperfusion (I/R).

RESULTS

Microhemodynamic Parameters and Systemic Leukocyte Counts. No statistically significant differences in microhemodynamic parameters and systemic leukocyte counts were detected among experimental groups receiving carboxyl-QDs, amine-QDs, or vehicle control (Supporting Information, Table S1).

Effect of Carboxyl-QDs and Amine-QDs on Postischemic Leukocyte Recruitment. Using *in vivo* microscopy on the mouse cremaster muscle (Figure 1A), steps of leukocyte recruitment were investigated. Figure 1 depicts a postcapillary venule in the postischemic cremaster tissue with leukocytes attached to the inner vessel wall and surrounded by extravasated leukocytes. As is well-known, surgical preparation of the cremaster muscle induced leukocyte rolling in postcapillary venules.[28,29] However, no significant differences in numbers of rolling leukocytes were observed among all experimental groups at baseline conditions prior to induction of ischemia as well as after 60 and 120 min of reperfusion (Figure 1B).

At baseline conditions, the number of firmly adherent leukocytes was low and did not differ among experimental groups (Figure 1C). As expected, the number of firmly adherent leukocytes ($13.7 \pm 1.5/10^4\ \mu m^2$) was significantly increased compared to sham-operated controls ($3.2 \pm 0.8/10^4\ \mu m^2$) after 30 min of ischemia and 60 min of reperfusion. Interestingly, application of carboxyl- ($25.7 \pm 6.8/10^4\ \mu m^2$) as well as of amine-QDs ($24.1 \pm 2.1/10^4\ \mu m^2$) at the onset of reperfusion resulted in a further increase in the number of adherent leukocytes in postischemic postcapillary venules. In contrast, numbers of adherent leukocytes were only

moderately increased in sham-operated animals upon administration of carboxyl- ($9.8 \pm 2.4/10^4$ μm^2) as well as of amine-QDs ($7.0 \pm 1.6/10^4$ μm^2) compared to sham-operated animals receiving vehicle. Similar results for postischemic firm adherence were obtained after 120 min of reperfusion (Figure 1C).

Prior to ischemia, only few extravasated leukocytes were detected within the perivascular tissue (Figure 1D). After 30 min of ischemia and 60 min of reperfusion, however, numbers of transmigrated cells were significantly increased ($29.4 \pm 3.9/10^4 \mu m^2$) compared to sham-operated mice ($10.7 \pm 1.3/10^4$ μm^2). Administration of amine-QDs led to a significant further increase ($49.1 \pm 2.1/10^4$ μm^2) in leukocyte transmigration.

In sham-operated mice, the numbers of extravasated leukocytes obtained after application of carboxyl-QDs ($22.4 \pm 4.3/10^4$ μm^2) and amine-QDs ($18.7 \pm 5.5/10^4$ μm^2) were significantly lower compared to all other groups except sham-operated animals receiving vehicle. Postischemic leukocyte transmigration after 120 min of reperfusion (Figure 1D) was found to be increased approximately 1.5-fold in all experimental groups compared to 60 min of reperfusion. Taken together, these data indicate that both amine- as well as carboxyl-QDs have an effect on leukocyte recruitment in the postischemic cremaster muscle preparation.

Phenotyping of Transmigrated Leukocytes. To identify the phenotype of transmigrated leukocytes, immunostaining of cremasteric tissue samples for CD45 (common leukocyte antigen), Gr-1 (neutrophils/monocytes), and F4/80 (monocytes/macrophages) was performed. In response to I/R, in all experimental groups, over 80% of transmigrated leukocytes were positive for Gr-1 and 10−20% of transmigrated leukocytes were positive for F4/80 (data not shown).

QD Localization in Postcapillary Venules of the Postischemic Cremasteric Tissue. According to our previously published results,[26,27] both amine- and carboxyl-QDs were detected in the bloodstream within seconds after application by *in vivo* fluorescence microscopy.

Within 2 min after injection, amine-QDs exhibited a stable and strong association with the vessel wall of postcapillary venules in the postischemic cremaster muscle (Figure 2A,B,I and Supporting Information movie S1). Amine-QDs were localized around similarly sized rounded structures at the vessel wall, best visible in images in which the upper part of the vessel was in focus (Figure 2I and Supporting Information movie S1). These structures were reminiscent of the cobblestone-like morphology of endothelial cells. Among the extravasated leukocytes migrating in the postischemic tissue, some cells contained amine-QDs (movie S1 and Figure 2J). In sham-operated animals, only a weak association of amine-QDs with the vessel wall was detected, localized in some distinct fluorescent spots (Figure 2C,D).

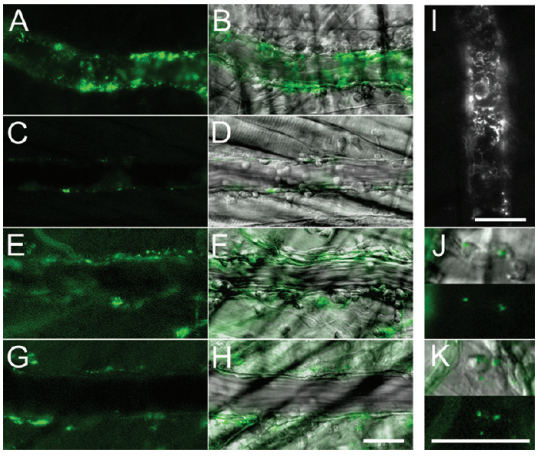

Figure 2. QD localization in postcapillary venules in the postischemic cremaster muscle. ***In vivo*** **fluorescence microscopy revealed localization of amine-QDs (A−D,I) and carboxyl-QDs (E−H) in postcapillary venules. The images displayed are taken from movies available in the Supporting Information and show representative localization patterns at 60 min after intra-arterial QD application (3 pmol/g of BW) at the onset of reperfusion after an ischemic period of 30 min (A,B,E,F,I) or sham operation (C,D,G,H). QD fluorescence is depicted in panels A, C, E, and G and merged with the corresponding bright-field images of the cremasteric tissue in panels B, D, F, and H. Fluorescence intensities between amine- and carboxyl-QD are not directly comparable. (J,K) Transmigrated leukocytes in the postischemic muscle tissue containing amine-QDs and carboxyl-QDs, respectively. Scale bar, 30 μm.**

Carboxyl-QDs showed a stable distribution along the vessel wall of postcapillary venules within a few minutes after application. Furthermore, carboxyl-QDs, but not amine-QDs, exhibited a strong association with capillaries and were localized in perivascular cells (Figure 2E,F and Supporting Information movie S2). These localization patterns did not differ in the cremaster muscles of mice undergoing ischemia/reperfusion or sham operation (Figure 2G,H). Carboxyl-QDs were also detected in transmigrated leukocytes in the postischemic tissue (Figure 2K). Essentially, the localization pattern of carboxyl-QDs in the postischemic cremaster muscle is comparable to the situation in healthy muscle tissue, as was reported previously.[26,27]

Quantification of QD Fluorescence at the Vessel Wall of Postcapillary Venules. Fluorescence intensity measurements in regions of interest covering the vessel walls of cremasteric postcapillary venules confirmed a strong association of these structures with amine-QDs (Figure 3). At 15 min after injection, amine-QD fluorescence intensities were approximately 2.5-fold higher (420 ± 57 au) compared to carboxyl-QDs (161 ± 10 au) intensity values, which were close to autofluorescence values (109 ± 5 au). Amine-QD fluorescence intensity at the vessel wall was significantly (214 ± 17 au) lower in sham-operated animals, while carboxyl-QD (184 ± 15 au) values were comparable to the postischemic QD fluorescence intensities given above. At 60 min after QD injection, amine-QD fluorescence at

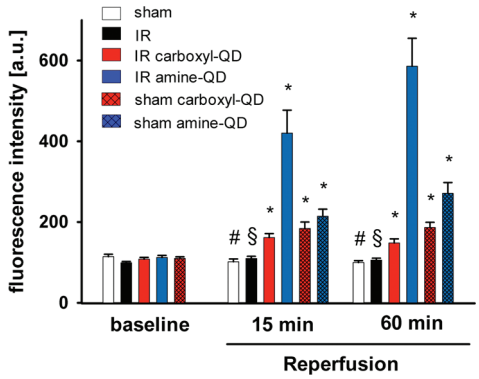

Figure 3. QD fluorescence intensities at the vessel wall of postcapillary venules in the postischemic cremaster muscle. QD fluorescence intensity values at the vessel wall are depicted. Images were acquired using a 12-bit grayscale intensity scale (*i.e.*, from 0 to 4095). Mean intensity values obtained are given. Although image acquisition times were carefully adjusted to allow for an optimal dynamic range, amine-QD saturation was inevitable for some pixels in the case of I/R. This was due to the presence of very bright amine-QD clusters. Note that the values are not background-corrected. Values for sham and I/R represent autofluorescence (mean ± SEM; $n = 12$ per group; *$p < 0.05$ *vs* all groups; #$p < 0.05$ *vs* all groups except IR, §$p < 0.05$ *vs* all groups except sham).

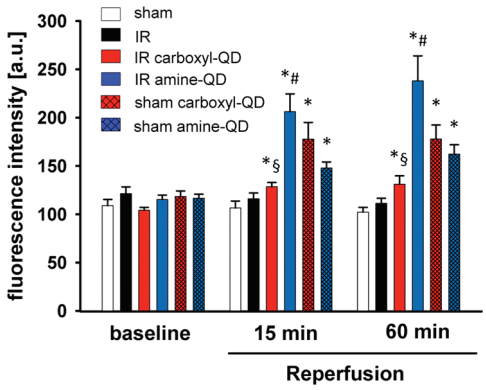

Figure 4. QD fluorescence intensities in postischemic tissue. QD fluorescence intensity values are depicted. Images were acquired using a 12-bit grayscale intensity scale (*i.e.*, from 0 to 4095). Mean intensity values obtained are given. Note that the values are not background-corrected. Values for sham and I/R represent autofluorescence (mean ± SEM; $n = 12$ per group; *$p < 0.05$ *vs* sham and I/R; #$p < 0.05$ *vs* sham amine-QDs, §$p < 0.05$ *vs* sham carboxyl-QDs).

the vessel wall was further increased (I/R amine-QDs 586 ± 69 au; sham amine-QDs 271 ± 27 au), whereas carboxyl-QD fluorescence intensities remained constant (I/R carboxyl-QDs 148 ± 10 au; sham carboxyl-QDs 186 ± 13 au). Although image acquisition times were carefully adjusted to allow for an optimal dynamic range, amine-QD pixel saturation, caused by very bright amine-QDs clusters at the postischemic vessel wall, was inevitable in the case of I/R.

Quantification of QD Fluorescence in Cremasteric Tissue. Next, QD fluorescence was determined in cremasteric tissue as a measure of QD extravasation (Figure 4). After 15 min of application, amine- (206 ± 18 au) and carboxyl-QD fluorescence (128 ± 4 au) in postischemic tissue as well as amine- and carboxyl-QDs fluorescence intensities (148 ± 6 and 178 ± 17 au) in control tissue were significantly enhanced compared to tissue autofluorescence (IR 116 ± 6 au; sham 107 ± 7 au). Most interestingly, 60 min upon injection of amine-QDs (238 ± 26 au), but not of carboxyl-QDs (131 ± 9 au), fluorescence intensities in postischemic tissue were further increased compared to control autofluorescence values (IR 111 ± 5 au; sham 102 ± 5 au), whereas both amine-QD (162 ± 10 au) and carboxyl-QD values (178 ± 15 au) were significantly enhanced in sham-treated animals.

Analysis of QD Association with Microvessels in the Postischemic Myocardium. Using two-photon microscopy, we investigated the association of amine- and carboxyl-QDs with microvessels in the postischemic heart muscle. Ligation of the left anterior coronary artery for 30 min induced local myocardial ischemia. Fifteen minutes after systemic application of QDs at the onset of reperfusion, two-photon imaging was performed. In the postischemic myocardium, amine-QDs displayed a very strong association with microvessel walls (Figure 5A,C,G). Amine-QD fluorescence intensities at the microvessel walls in the postischemic myocardium, determined in regions of interest, were 2512 ± 644 au. In nonischemic areas, however, amine-QDs exhibited a very weak association with microvessels (85 ± 24 au) (Figure 5B,G), resulting in images with low signal-to-background ratios. As was previously reported by our group,[26] carboxyl-QDs exhibited a clear colocalization with microvessel walls in the nonischemic (303 ± 31 au) (Figure 5E,G) as well as in postischemic (604 ± 104 au) (Figure 5D,F,G) heart tissue.

Electron Microscopy. Electron microscopy was employed to further investigate the localization of QDs in the vessel wall of postcapillary venules of postischemic cremasteric tissue (Figure 6). As reported previously, elliptical-shaped QDs were only unambiguously identified after omitting the standard counterstain (uranyl acetate and lead).[27] Therefore, the image contrast is predominantly caused by osmified membrane lipids. As depicted, carboxyl-QDs were detected in caveolae and in endosomes/multivesicular bodies of endothelial cells, thus indicating caveolae-mediated endocytosis (Figure 6B). Carboxyl-QD-containing caveolae were mostly found at the luminal side of the endothelial cells, often connected with the plasma membrane. The cytoplasm of these cells was devoid of carboxyl-QDs. In contrast, amine-QDs were never found inside endothelial cells (Figure 6C,D). Interestingly, amine-QDs were predominantly clustered with extracellular membrane vesicles, with a size of approximately 50 nm. These clusters were localized between endothelial cells at the vessel walls.

On the basis of their size and vesicular structure, these membrane fragments were identified as endogenous microparticles (MPs). Endogenous MPs

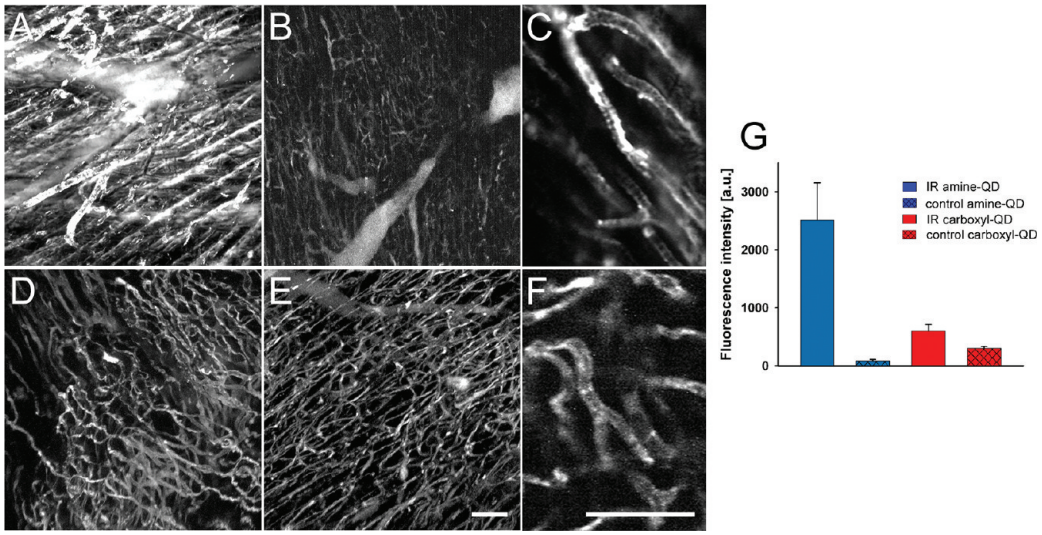

Figure 5. *Ex vivo* two-photon microscopy of QDs in the postischemic heart muscle. Mice received a bolus injection of amine- or carboxyl-QDs [3 pmol/g BW] *via* a venous catheter at the onset of reperfusion after an ischemic period of 30 min. After 15 min of reperfusion, hearts were dissected and thoroughly flushed with saline. Representative maximum intensity projections covering 150 μm (*z*-distance 5 μm) of ischemic heart muscle containing (A) amine-QDs or carboxyl-QDs (D) are shown. (B,E) Control heart tissue containing amine- or carboxyl-QDs, respectively. Single *z*-planes demonstrate the association of amine- (C) as well as carboxyl-QDs (F) with microvessel walls in the postischemic myocardium. Fluorescence intensities are not directly comparable. (G) Mean QD fluorescence intensities at microvessel walls (n = 12) were determined in eight individual *z*-stacks (mean ± SEM; scale bar, 50 μm).

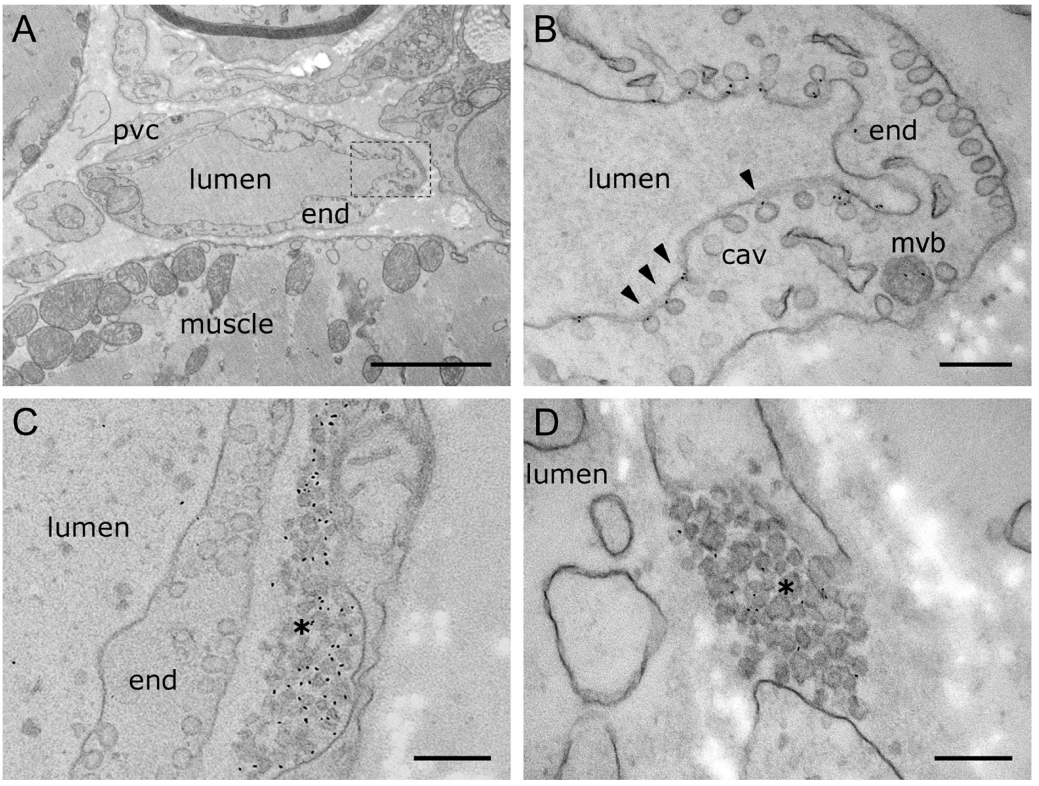

Figure 6. Electron microscopy. Transmission electron microscopy was performed on ultrathin cross sections of cremasteric tissue 60 min upon application of QDs. Contrast of the tissue results from postfixation of lipids with OsO_4; only representative images are shown. (A) Overview on a cross-sectioned postcapillary venule: the endothelial cell layer (end) is bounded by perivascular cells (pvc) and surrounded by muscle tissue. Dashed inset is shown in (B). This high magnification of an endothelial cell layer shows single carboxyl-QDs (arrowheads) during uptake in caveolae (cav). Carboxyl-QDs also localize in multivesicular bodies (mvb). (C,D) Typical distribution of amine-QDs. Amine-QDs mainly associate with endogenous microparticles (asterisk) which were found clustered between endothelial cells. These aggregates leak out of the vessel *via* cellular gaps which are formed as an effect of ischemia (D). Microparticle size was approximately 50 nm. Note that endothelial cells are devoid of amine-QDs. (A) Scale bar represents 2 μm. (B–D) Scale bars represent 200 nm.

are described as a heterogeneous population of small plasma membrane structures (0.05−1 μm) circulating in the blood, derived from platelets, erythrocytes, white blood cells, and endothelial cells.[30,31] IR induces dissociation of endothelial cell junctions and cytoskeleton contraction, leading to the formation of endothelial gaps.[17,32] Clusters of amine-QDs with MPs were localized in such vascular gaps and apparently tended to leak out of the vessel lumen through these structures (Figure 6D). Considerably more MP aggregates were found in vascular gaps of postischemic cremasteric tissue of animals receiving amine-QDs compared to mice receiving carboxyl-QDs. Moreover, no association of carboxyl-QDs with MPs was detected in these samples.

Interestingly, clusters of amine-QDs with MPs were found only in the immediate vicinity of vascular gaps, suggesting that structures of the interstitial matrix, such as collagen fibers, which are visible in the TEM images, act as a barrier to prevent further distribution of clusters of amine-QDs with MPs into the tissue.

FACS Analysis. The association of amine-QDs with MPs at microvessel walls prompted us to ask whether this interaction occurs only in postischemic tissue or happens in principle after injection of QDs into the blood circulation. Therefore, we used FACS analysis on blood samples of healthy mice obtained 10 min upon injection of QDs to further investigate QD association with MPs in the circulating blood (Supporting Information Figure 1). MPs were isolated from plasma samples by differential centrifugation and labeled with annexin V for identification. As obtained by FACS analysis, 12.1 ± 2.1% of annexin-V-stained MPs were associated with amine-QDs, whereas the percentage of carboxyl-QDs associated with annexin-V-positive MPs (0.4 ± 0.2%) matched the blank values (0.8 ± 0.1%).

DISCUSSION

Even though the functional consequences of deprivation of blood supply to the tissue are well-known for many years, the cardiovascular diseases induced by local or systemic ischemia remain the main cause of death in Europe and the Unites States.[17] Therefore, new therapeutics and diagnostic tools to improve the outcome of ischemia-reperfusion (I/R) injury are currently being developed, including the utilization of different nanomaterials.[7−11] It is widely recognized that the microvasculature, particularly the endothelial cells, is very vulnerable to the deleterious consequences of I/R. Leukocyte−endothelial cell interactions, leukocyte extravasation, increase of microvascular permeability, and enhanced oxidant production in postcapillary venules are hallmarks of the acute inflammatory response induced by I/R.[17]

Recent research shows that nanoparticles can stimulate and/or suppress immune responses, and that their compatibility with the immune system is largely determined by their surface chemistry.[33] Therefore, we investigated the fate and effects of surface-modified QDs in the postischemic microvasculature. To our knowledge, our *in vivo* study is the first to demonstrate that I/R-elicited leukocyte recruitment is amplified in the presence of nanoparticles. We found that the surface chemistry of nanomaterials strongly affects their localization in microvessels in the postischemic skeletal and heart muscle tissue. We speculate that both the observed differences in the localization of QDs and their association with endogenous MPs are causal for the impact on leukocyte recruitment.

Interestingly, we found only a slight increase in carboxyl-QD fluorescence intensities in the interstitial postischemic cremasteric tissue, whereas carboxyl-QD fluorescence was significantly enhanced under sham conditions. This coincides with the observation that carboxyl-QDs were strictly localized in caveolae of endothelial cells as we have shown in this study for postischemic and control tissues, thereby confirming our recently published results concerning the endothelial localization of carboxyl-QDs.[26,27] Intriguingly, carboxyl-QD-containing caveolae were mostly found at the luminal side of endothelial cells, often connected with the plasma membrane. Pinching off of endocytic vesicles/caveolae from the plasma membrane and vesicle transport in the cells are ATP-dependent processes involving the action of GTPases and molecular motors.[34] Energy depletion, here as a result of the ischemic period, might thus inhibit vesicle transport, as was shown for uptake and transport of nanocomplexes by epithelial cells.[35] This might argue for a mainly active transport of carboxyl-QDs by transcytosis, a mechanism particularly prominent in vascular endothelial cells, mediating bidirectional exchange of macromolecules between blood and interstitium,[36] rather than diffusion of carboxyl-QDs through vascular gaps. On the contrary, interstitial amine-QD fluorescence intensities were highest in postischemic tissue and hence in accordance with the extravasation of amine-QDs due to enhanced microvascular permeability. The specific uptake of carboxyl-QDs in caveolae of endothelial cells could be mediated by surface-bound biomolecules recognized by receptors localized on caveolae or their precursors (uncoated pits) since it is well-established that proteins and other biomolecules account for the biological identity of nanoparticles.[37,38] Taken together, the localization patterns of carboxyl-QDs were not altered under the pathophysiologic conditions of I/R and matched their localization under more physiologic conditions.[27]

On the other hand, the localization of amine-QDs in the postischemic tissue was strikingly different from control tissue. TEM microscopy revealed that amine-QDs at microvessel walls were always associated with MPs and exclusively localized extracellularly. FACS analysis of annexin-V-labeled MPs demonstrated that the association of amine-QDs with MPs is not dependent on I/R but occurs also very rapidly, and specific, in the circulating blood of healthy animals.

Endogenous MPs are considered to be membrane nanofragments (0.05−1 μm) with procoagulant and proinflammatory properties, thus acting as circulating ubiquitous bioeffectors. MPs are present in the bloodstream of healthy as well as diseased individuals. Moreover, they have been described to take part in vascular function, acting as vectors for intercellular exchange of biologic information, thus influencing endothelial modifications, angiogenesis, or differentiation.[39,40] MPs have been detected in ischemic muscle tissue where they are thought to promote vasculogenesis.[41] Most interestingly, it was demonstrated that numbers of circulating, procoagulant MPs were more elevated in patients with acute myocardial infarction than in patients with stable coronary artery disease. Moreover, shortly after myocardial infarction, there was an initial decrease of MP−platelet aggregates compared to stable patients, possibly because these aggregates are sequestered in the infarcted vessel, as discussed by the authors.[42−44]

In this context, we could clearly demonstrate that aggregates of MPs with amine-QDs were localized in considerable amounts between and in close proximity to endothelial gaps at microvessel walls. Furthermore, we detected, albeit to a lesser extent, MPs at the same localizations in both postischemic control and carboxyl-QD-containing cremaster muscle samples. Although it is well-known that local tissue apoptosis is induced in ischemic tissues[22,45] and that MPs are shed from apoptotic or activated (endothelial) cells,[30] our data favor the hypothesis that the association of amine-QDs with MPs occurs in the circulating blood and that these clusters are subsequently sequestered to vascular gaps. MP size at these localizations was noteworthy homogeneous and with approximately 50 nm at the lower end of the described size range for MPs. This size distribution could be facilitated by sheering of MPs as they access vascular gaps or due to a size-dependent enrichment caused by blood rheology. The bloodborne MPs, which are detectable by annexin V staining and FACS analysis, are due to restrictions of the technique employed, most likely bigger than 0.5 μm, as was currently discussed by Furie *et al.*[46] Annexin V binds with high affinity to the negatively charged headgroup of phosphatidylserine,[47] which is exposed at the outer membrane surface of MPs.[42] The interaction of amine-QDs with the negatively charged membrane could be mediated by electrostatic interactions which have been reported to be responsible for the initial interaction between cationic macromolecules and the negatively charged cell membrane.[48] However, we were not able to detect any association of amine-QDs with the membrane of endothelial cells, which might imply that the association of amine-QDs with MPs is mediated in a more specific manner. This issue as well as the cellular origin of the MPs clearly need to be addressed in further studies.

The cremaster muscle preparation is a well-defined and widely used model system to investigate mode and mechanisms of leukocyte recruitment.[24,29,49] Model-inherent properties include P-selectin-dependent leukocyte rolling, followed by slight leukocyte adhesion and transmigration due to the surgical preparation. Mast cells do not contribute to this basal inflammatory response,[50] which is very mild compared to inflammation obtained after application of inflammatory mediators such as PAF and MIP-1-alpha or after I/R.[24,29,49,51,52] We have previously reported that carboxyl-QD-elicited leukocyte recruitment depends on mast cell activation and the expression of endothelial cell adhesion proteins.[27]

The acute inflammatory response, induced by I/R, is associated with the release of soluble proinflammatory mediators by tissue macrophages or mast cells that reside immediately adjacent to postcapillary venules where they amplify the inflammatory response to I/R resulting in the activation of the endothelium.[53,54] We found that the I/R-elicited leukocyte adhesion was amplified after application of both carboxyl- and amine-QDs. Interestingly enough, only amine-QDs significantly increased I/R-elicited leukocyte transmigration and thus aggravated the inflammatory response. This effect could well be facilitated by recruited MPs since they are known to affect inflammation in several ways.[39,42] *In vitro*, the stimulation of endothelial cells by MPs results in cytokine release and expression of adhesion molecules.[55] MPs promote interactions between leukocytes and endothelium *in vivo* by participating in the release of several endothelial or monocytic cytokines.[56]

CONCLUSION

Taken together, these findings demonstrate that both the surface chemistry of QDs and the underlying tissue conditions (I/R) strongly affect their fate *in vivo*, that is, their cellular and noncellular interactions in microvessels, their association with endogenous MPs, and their potential to modify inflammatory processes. Thus, this study strongly corroborates the view that both the surface chemistry of nanomaterials and the physiological state of the tissue are crucial for the behavior of nanomaterials *in vivo*. This also warrants further studies in which other surface chemistries than the ones used here are investigated.

MATERIALS AND METHODS

Animals. Male C57BL/6 mice at the age of 10−12 weeks were purchased from Charles River (Sulzfeld, Germany). Animals were housed under conventional conditions with free access to food and water. All experiments were performed according to German legislation for the protection of animals.

Quantum Dots. Qdot ITK carboxyl and Qdot ITK amine (PEG) quantum dots (655 nm fluorescence peak emission) were purchased from Invitrogen Corporation (Karlsruhe, Germany). These QDs consist of a semiconductor CdSe core encapsulated with a ZnS shell and an additional layer of polyethylene glycol with an amine coating (amine-QDs) or carboxyl functions solely (carboxyl-QDs). The PEG coating itself consists of short oligomers with a molecular weight of 1−3 kDa. The physical characterization of QDs was previously performed in our laboratory and has been published.[26,27] Prior to use, QDs were resuspended to a final volume of 100 μL in sterile 0.9% NaCl at a concentration of 0.8 μM, thoroughly vortexed, and injected intra-arterially.

Surgical Procedure. The surgical preparation was performed as described by Baez with minor modifications.[49] Briefly, mice were anesthetized using a ketamine/xylazine mixture (100 mg/kg ketamine and 10 mg/kg xylazine), administrated by i.p. injection. The left femoral artery was cannulated in a retrograde manner for administration of QDs and microspheres. The right cremaster muscle was exposed through a ventral incision of the scrotum. The muscle was opened ventrally in a relatively avascular zone, using careful electrocautery to stop any bleeding, and spread over the pedestal of a custom-made microscopy stage. Epididymis and testicle were detached from the cremaster muscle and placed into the abdominal cavity. Throughout the procedure as well as after surgical preparation during *in vivo* microscopy, the muscle was superfused with warm buffered saline.

***In Vivo* Microscopy.** For *in vivo* microscopy, an AxioTech-Vario 100 microscope (Zeiss MicroImaging GmbH, Göttingen, Germany) equipped with a LED light source (Zeiss Colibri) for fluorescence epi-illumination was used. For QD excitation and transillumination, the 470 nm LED module (exposure time 150 ms) and the 625 nm LED module (exposure time 10 ms) were used in a fast switching mode, respectively. Light was directed onto the specimen *via* filter set 62 HE (Zeiss MicroImaging GmbH) fitted with dichroic and emission filters [TFT 495 + 610 (HE); TBP 527 + LP615 (HE)]. Microscopic images were obtained with a water dipping objective (20×, NA 0.5) and acquired with an AxioCam Hsm camera and Axiovision 4.8 software. Oblique illumination was obtained by positioning a mirroring surface (reflector) directly below the specimen and tilting its angle relative to the horizontal plane. The reflector consisted of a round cover glass (thickness, 0.19−0.22 mm; diameter, 11.8 mm), which was coated with aluminum vapor (NiWe Decor GmbH, Kaufbeuren, Germany) and brought into direct contact with the overlying specimen as described previously.[29] For measurement of centerline blood flow velocity, green fluorescent microspheres (2 μm diameter, Invitrogen) were injected *via* the femoral artery catheter, and their passage through the vessels of interest was recorded (filter set 62 HE, LED 470 nm).

Experimental Groups. Animals were assigned randomly to the following groups: sham-operated mice without ischemia as well as mice undergoing I/R (30/120 min) (n = 6 per group) receiving vehicle, carboxyl-QDs, or and amine-QDs.

Experimental Protocols. For the analysis of postischemic leukocyte responses, five postcapillary vessel segments in a central area of the spread-out cremaster muscle were randomly chosen among those that were at least 150 μm away from neighboring postcapillary venules and did not branch over a distance of at least 150 μm. After having obtained baseline recordings of leukocyte rolling, firm adhesion, and transmigration in all five vessel segments, ischemia was induced by clamping all supplying vessels at the basis of the cremaster muscle using a vascular clamp (Martin, Tuttlingen, Germany). Stagnancy of blood flow was then verified by *in vivo* microscopy. In sham-operated animals, the vascular clamp was closed, instantly unclosed, and removed. After 30 min of ischemia, the vascular clamp was removed and reperfusion was restored for 120 min. At the onset of reperfusion, mice (n = 6 each group) received vehicle, carboxyl-QDs, or amine-QDs (3 pmol/g BW) as a bolus by intra-arterial injection. Measurements, which took about 5 min, were repeated at 60 and 120 min after onset of reperfusion. After having obtained recordings of leukocyte recruitment parameters, blood flow velocity was determined as described previously.[57] After *in vivo* microscopy, tissue samples of the cremaster muscle were prepared for immunohistochemistry and electron microscopy. Blood samples were collected by cardiac puncture for the determination of systemic leukocyte counts using a Coulter ACT counter (Coulter Corp., Miami, FL). Anesthetized animals were then euthanized by an intra-arterial pentobarbital overdose (Narcoren; Merial, Hallbergmoos, Germany).

Quantification of Leukocyte Kinetics, Microhemodynamic Parameters, and QD Fluorescence. For off-line analysis of parameters describing the sequential steps of leukocyte extravasation, Axiovision 4.8 software was used. Rolling leukocytes were defined as those moving slower than the associated blood flow and quantified during 30 s. Firmly adherent cells were determined as those resting in the associated blood flow for more than 30 s and related to the luminal surface per 100 μm vessel length. Transmigrated cells were counted in regions of interest (ROI), covering 75 μm on both sides of a vessel over 100 μm vessel length and are presented per 10^4 mm^2 tissue area. From consecutive movie frames of single fluorescent microspheres, centerline blood flow velocity was determined. From measured vessel diameters and centerline blood flow velocity, apparent wall shear stress was calculated, assuming a parabolic flow velocity profile over the vessel cross section as described previously.[57]

For determination of QD fluorescence at the vessel walls of postcapillary venules, regions of interest (ROI) covering 100 μm length of both visible vessel walls were analyzed in single movie frames in which the transverse section of the analyzed vessel was in the focal plane. Vessel walls were identified in the corresponding transillumination image. QD fluorescence intensity values in these ROIs were measured, and mean intensity values are given. Images were acquired using a 12-bit grayscale intensity scale (*i.e.*, from 0 to 4095). Accordingly, interstitial QD fluorescence was determined in six randomly selected ROIs (50 × 50 μm^2), localized 50 μm distant from the postcapillary venule under investigation. Twelve microvessels were analyzed per experimental group. Analysis was done using ImageJ software (National Institutes of Health, Bethesda, MD).

Immunohistochemistry. To determine the phenotype of transmigrated leukocytes, immunostaining of paraffin-embedded serial tissue sections of the cremaster muscle was performed. Sections were incubated with primary rat anti-mouse Gr-1, anti-CD45 (BD Biosciences, San Jose, CA), or anti-F4/80 (Serotec, Oxford, UK) IgG antibodies. The paraffin sections were stained with commercially available immunohistochemistry kits (Gr-1, CD45, Super Sensitive Link-Label IHC detection system, BioGenex, San Ramon, CA; F4/80, Vectastain ABC kit, Vector Laboratories, Burlingame, CA), obtaining an easily detectable reddish or brownish end product, respectively. Counterstaining was performed with Mayer's hemalaun. The number of extravascularly localized Gr-1-, CD45-, or F4/80-positive cells was quantified by light microscopy (objective magnification 40×) on two sections (10 observation fields per section) from six animals in a blinded manner. The number of transmigrated Gr-1-positive cells (neutrophils/monocytes) and F4/80-positive cells (monocytes/macrophages) is expressed as the percentage of total CD45-positive leukocytes.

Electron Microscopy. The cremaster muscle was initially fixed *in situ* in 1% PFA, 0.1 M cacodylate buffer, pH 7.4 and, after dissection, finally fixed in 2% PFA, 2% glutaraldehyde in 0.1 M cacodylate buffer, pH 7.4 for 2−3 h at room temperature. The specimens were postfixed in 1% OsO_4, containing 1.5% potassium cyanoferrate and embedded after dehydration in Epon. Ultrathin (70 nm) sections of the sample were cut in serial sections (Leica-UC6 ultramicrotome, Vienna, Austria). Several sections were counterstained with uranyl acetate and lead, and some of the sections were not counterstained. The samples were analyzed at 80 kV on a FEI-Tecnai 12 electron microscope (FEI, Eindhoven, The Netherlands). QDs were localized in the unstained sections. The consecutive stained section was used to identify the cellular organelle. Images were acquired using a CCD camera (Megaview, Olympus-SIS, Muenster).

Mouse Model of Myocardial Ischemia/Reperfusion. Mice were anesthetized with ketamine (75 mg/kg) and xylazine (15 mg/kg) and ventilated *via* a Hugo Sachs Harvard Apparatus respirator (Hugstetten, Germany). The body temperature was maintained at 37 °C with a heated blanket. After ligation of the left anterior descending coronary artery for 30 min, thereby inducing local

myocardial ischemia, QDs (3 pmol/g BW) were infused into the external jugular vein at the onset of reperfusion. After 15 min of reperfusion, isolated hearts (n = 2 per group) were thoroughly flushed with isothermic saline solution, dissected, and placed on a silica matrix, plainly fixed with cannulae and superfused with 0.9% NaCl solution.

Two-Photon Microscopy of QD Distribution in Heart Muscle Tissue. Two-photon microscopy on ischemic as well as control areas of the obtained heart muscle tissues was performed on a TriM-Scope (LaVision Biotec, Bielefeld, Germany) built around an Olympus BX 51 microscope (Olympus, Hamburg, Germany) and equipped with a tunable Ultra II Ti:sapphire laser (Coherent, Dieburg, Germany) and an optical parametric oscillator (Chameleon OPO; APE, Berlin, Germany) which is pumped by the Ti:sapphire laser. An Olympus XLUMPlanFI 20/0.95W water immersion objective was used. Excitation wavelength was 1150 nm. QD emission was detected at 635−695 nm using a Hamamatsu H6780-20 photomultiplier tube and a 700 nm short pass filter. Four optical sections at high resolution (500 × 500 μm with 1225 × 1225 pixels) were recorded per ischemic or control area at 5 μm distances using the same settings for all samples analyzed. The z-stacks covering 250 μm were projected and further processed using ImageJ software (National Institutes of Health, Bethesda, MD). Mean fluorescence intensities were determined in regions of interest covering 100 μm length of microvessel walls. Twelve microvessels were analyzed per optical section.

Flow Cytometric Analysis of QD Association with Microparticles. For purification and flow cytometric analysis of microparticles, a published protocol was adapted.[58] Blood samples obtained by cardial puncture 10 min after intra-arterial injection of QDs (3 pmol/g BW) were centrifuged at 1550g at room temperature. Then, 250 μL of the obtained plasma was further centrifuged at 17500g (RT) to get microparticle pellets. These pellets were resuspended in Apo buffer (10 mmol/L Hepes, 5 mmol/L KCl, 1 mmol/L $MgCl_2$, and 136 mmol/L NaCl; pH 7.4) and recentrifuged. The pellets were resuspended in 20 μL of Apo buffer; subsequently 140 μL of Apo buffer containing 2.5 mmol/L $CaCl_2$ and 20 μL of microparticle-free normal mouse serum were added and incubated for 15 min at room temperature. In order to identify the microparticles, 5 μL of Alexa488-labeled annexin V (Invitrogen) was added to 130 μL of the sample and incubated for 15 min in the dark. Stained microparticles were analyzed on a flow cytometer (FACSort, Becton Dickinson, Franklin Lakes, NJ). Microparticles were identified on forward scatter, sideward scatter, and binding of annexin V. Alexa488-labeled annexin V and QDs were excited at 488 nm and detected at 515−545 nm (channel FL-1) and 650 nm (channel FL-3), respectively. Approximately 10 000 gated events were collected in each analysis.

Statistics. Data analysis was performed with a statistical software package (SigmaStat for Windows, SPSS Inc., Chicago, IL). The ANOVA on ranks test, which includes tests for normality and equal variance of the data, was performed. When p values <0.05 were detected by ANOVA, then the appropriate posthoc test (Student−Newman−Keuls) for all pairwise multiple comparisons was used to estimate the stochastic probability in intergroup comparisons. Mean values and SEM are given. The p values <0.05 were considered significant.

Conflict of Interest: The authors declare no competing financial interest.

Acknowledgment. This work was supported by the BioImaging Network Munich and by grants from the Friedrich-Baur-Stiftung (to M.R.) and the European Commission (STREP "NANOSH" to F.K.). The authors thank A. Schropp and G. Adams for technical assistance.

Supporting Information Available: Microhemodynamic parameters and systemic leukocyte counts, *in vivo* fluorescence microscopy movies, and FACS analysis of endogenous MPs. This material is available free of charge *via* the Internet at http://pubs.acs.org.

REFERENCES AND NOTES

1. Nel, A.; Xia, T.; Madler, L.; Li, N. Toxic Potential of Materials at the Nanolevel. *Science* **2006**, *311*, 622–627.
2. Xia, Y. Nanomaterials at Work in Biomedical Research. *Nat. Mater.* **2008**, *7*, 758–760.
3. Gao, X.; Cui, Y.; Levenson, R. M.; Chung, L. W.; Nie, S. *In Vivo* Cancer Targeting and Imaging with Semiconductor Quantum Dots. *Nat. Biotechnol.* **2004**, *22*, 969–976.
4. Medintz, I. L.; Uyeda, H. T.; Goldman, E. R.; Mattoussi, H. Quantum Dot Bioconjugates for Imaging, Labelling and Sensing. *Nat. Mater.* **2005**, *4*, 435–446.
5. Peer, D.; Karp, J. M.; Hong, S.; Farokhzad, O. C.; Margalit, R.; Langer, R. Nanocarriers as an Emerging Platform for Cancer Therapy. *Nat. Nanotechnol.* **2007**, *2*, 751–760.
6. Zintchenko, A.; Susha, A. S.; Concia, M.; Feldmann, J.; Wagner, E.; Rogach, A. L.; Ogris, M. Drug Nanocarriers Labeled with Near-Infrared-Emitting Quantum Dots (Quantoplexes): Imaging Fast Dynamics of Distribution in Living Animals. *Mol. Ther.* **2009**, *17*, 1849–1856.
7. Galagudza, M. M.; Korolev, D. V.; Sonin, D. L.; Postnov, V. N.; Papayan, G. V.; Uskov, I. S.; Belozertseva, A. V.; Shlyakhto, E. V. Targeted Drug Delivery into Reversibly Injured Myocardium with Silica Nanoparticles: Surface Functionalization, Natural Biodistribution, and Acute Toxicity. *Int. J. Nanomed.* **2010**, *5*, 231–237.
8. He, N.; Wang, T.; Jiang, L.; Wang, D.; Hu, Y.; Zhang, L. Therapy for Cerebral Ischemic Injury with Erythropoietin-Containing Nanoparticles. *J. Nanosci. Nanotechnol.* **2010**, *10*, 5320–5323.
9. Kim, J.; Cao, L.; Shvartsman, D.; Silva, E. A.; Mooney, D. J. Targeted Delivery of Nanoparticles to Ischemic Muscle for Imaging and Therapeutic Angiogenesis. *Nano Lett.* **2011**, *11*, 694–700.
10. McAteer, M. A.; Akhtar, A. M.; von Zur Muhlen, C.; Choudhury, R. P. An Approach to Molecular Imaging of Atherosclerosis, Thrombosis, and Vascular Inflammation Using Microparticles of Iron Oxide. *Atherosclerosis* **2010**, *209*, 18–27.
11. Oh, K. S.; Song, J. Y.; Yoon, S. J.; Park, Y.; Kim, D.; Yuk, S. H. Temperature-Induced Gel Formation of Core/Shell Nanoparticles for the Regeneration of Ischemic Heart. *J. Controlled Release* **2010**, *146*, 207–211.
12. Nemmar, A.; Hoet, P. H.; Vanquickenborne, B.; Dinsdale, D.; Thomeer, M.; Hoylaerts, M. F.; Vanbilloen, H.; Mortelmans, L.; Nemery, B. Passage of Inhaled Particles into the Blood Circulation in Humans. *Circulation* **2002**, *105*, 411–414.
13. Oberdorster, G.; Maynard, A.; Donaldson, K.; Castranova, V.; Fitzpatrick, J.; Ausman, K.; Carter, J.; Karn, B.; Kreyling, W.; Lai, D.; *et al.* Principles for Characterizing the Potential Human Health Effects from Exposure to Nanomaterials: Elements of a Screening Strategy. *Part. Fibre Toxicol.* **2005**, *2*, 8.
14. Oberdorster, G.; Oberdorster, E.; Oberdorster, J. Nanotoxicology: An Emerging Discipline Evolving from Studies of Ultrafine Particles. *Environ. Health Perspect.* **2005**, *113*, 823–839.
15. Peters, A.; Dockery, D. W.; Muller, J. E.; Mittleman, M. A. Increased Particulate Air Pollution and the Triggering of Myocardial Infarction. *Circulation* **2001**, *103*, 2810–2815.
16. Cozzi, E.; Hazarika, S.; Stallings, H. W., III; Cascio, W. E.; Devlin, R. B.; Lust, R. M.; Wingard, C. J.; Van Scott, M. R. Ultrafine Particulate Matter Exposure Augments Ischemia-Reperfusion Injury in Mice. *Am. J. Physiol. Heart Circ. Physiol.* **2006**, *291*, H894–903.
17. Carden, D. L.; Granger, D. N. Pathophysiology of Ischaemia-Reperfusion Injury. *J. Pathol.* **2000**, *190*, 255–266.
18. Harris, A. G.; Leiderer, R.; Peer, F.; Messmer, K. Skeletal Muscle Microvascular and Tissue Injury after Varying Durations of Ischemia. *Am. J. Physiol.* **1996**, *271*, H2388–2398.
19. Jolly, S. R.; Kane, W. J.; Hook, B. G.; Abrams, G. D.; Kunkel, S. L.; Lucchesi, B. R. Reduction of Myocardial Infarct Size by Neutrophil Depletion: Effect of Duration of Occlusion. *Am. Heart J.* **1986**, *112*, 682–690.
20. Romson, J. L.; Hook, B. G.; Kunkel, S. L.; Abrams, G. D.; Schork, M. A.; Lucchesi, B. R. Reduction of the Extent of Ischemic Myocardial Injury by Neutrophil Depletion in the Dog. *Circulation* **1983**, *67*, 1016–1023.

21. Gasser, O.; Schifferli, J. A. Activated Polymorphonuclear Neutrophils Disseminate Anti-inflammatory Microparticles by Ectocytosis. *Blood* **2004**, *104*, 2543–2548.
22. Khandoga, A.; Kessler, J. S.; Meissner, H.; Hanschen, M.; Corada, M.; Motoike, T.; Enders, G.; Dejana, E.; Krombach, F. Junctional Adhesion Molecule-A Deficiency Increases Hepatic Ischemia-Reperfusion Injury Despite Reduction of Neutrophil Transendothelial Migration. *Blood* **2005**, *106*, 725–733.
23. Ley, K. Healing Without Inflammation? *Am. J. Physiol. Regul. Integr. Comp. Physiol.* **2003**, *285*, R718–719.
24. Ley, K.; Laudanna, C.; Cybulsky, M. I.; Nourshargh, S. Getting to the Site of Inflammation: The Leukocyte Adhesion Cascade Updated. *Nat. Rev. Immunol.* **2007**, *7*, 678–689.
25. Nourshargh, S.; Hordijk, P. L.; Sixt, M. Breaching Multiple Barriers: Leukocyte Motility through Venular Walls and the Interstitium. *Nat. Rev. Mol. Cell. Biol.* **2010**, *11*, 366–378.
26. Praetner, M.; Rehberg, M.; Bihari, P.; Lerchenberger, M.; Uhl, B.; Holzer, M.; Eichhorn, M. E.; Furst, R.; Perisic, T.; Reichel, C. A.; *et al.* The Contribution of the Capillary Endothelium to Blood Clearance and Tissue Deposition of Anionic Quantum Dots *in Vivo*. *Biomaterials* **2010**, *31*, 6692–6700.
27. Rehberg, M.; Praetner, M.; Leite, C. F.; Reichel, C. A.; Bihari, P.; Mildner, K.; Duhr, S.; Zeuschner, D.; Krombach, F. Quantum Dots Modulate Leukocyte Adhesion and Transmigration Depending on Their Surface Modification. *Nano Lett.* **2010**, *10*, 3656–3664.
28. Kunkel, E. J.; Jung, U.; Bullard, D. C.; Norman, K. E.; Wolitzky, B. A.; Vestweber, D.; Beaudet, A. L.; Ley, K. Absence of Trauma-Induced Leukocyte Rolling in Mice Deficient in Both P-Selectin and Intercellular Adhesion Molecule 1. *J. Exp. Med.* **1996**, *183*, 57–65.
29. Mempel, T. R.; Moser, C.; Hutter, J.; Kuebler, W. M.; Krombach, F. Visualization of Leukocyte Transendothelial and Interstitial Migration Using Reflected Light Oblique Transillumination in Intravital Video Microscopy. *J. Vasc. Res.* **2003**, *40*, 435–441.
30. Morel, O.; Jesel, L.; Freyssinet, J. M.; Toti, F. Cellular Mechanisms Underlying the Formation of Circulating Microparticles. *Arterioscler., Thromb., Vasc. Biol.* **2011**, *31*, 15–26.
31. Tushuizen, M. E.; Diamant, M.; Sturk, A.; Nieuwland, R. Cell-Derived Microparticles in the Pathogenesis of Cardiovascular Disease: Friend or Foe? *Arterioscler., Thromb., Vasc. Biol.* **2011**, *31*, 4–9.
32. Kumar, P.; Shen, Q.; Pivetti, C. D.; Lee, E. S.; Wu, M. H.; Yuan, S. Y. Molecular Mechanisms of Endothelial Hyperpermeability: Implications in Inflammation. *Expert Rev. Mol. Med.* **2009**, *11*, e19.
33. Dobrovolskaia, M. A.; Germolec, D. R.; Weaver, J. L. Evaluation of Nanoparticle Immunotoxicity. *Nat. Technol.* **2009**, *4*, 411–414.
34. Soldati, T.; Schliwa, M. Powering Membrane Traffic in Endocytosis and Recycling. *Nat. Rev. Mol. Cell. Biol.* **2006**, *7*, 897–908.
35. Mao, S.; Germershaus, O.; Fischer, D.; Linn, T.; Schnepf, R.; Kissel, T. Uptake and Transport of PEG-Graft-Trimethyl-Chitosan Copolymer-Insulin Nanocomplexes by Epithelial Cells. *Pharm. Res.* **2005**, *22*, 2058–2068.
36. Simionescu, M.; Popov, D.; Sima, A. Endothelial Transcytosis in Health and Disease. *Cell Tissue Res.* **2009**, *335*, 27–40.
37. Aggarwal, P.; Hall, J. B.; McLeland, C. B.; Dobrovolskaia, M. A.; McNeil, S. E. Nanoparticle Interaction with Plasma Proteins as it Relates to Particle Biodistribution, Biocompatibility and Therapeutic Efficacy. *Adv. Drug Delivery Rev.* **2009**, *61*, 428–437.
38. Rocker, C.; Potzl, M.; Zhang, F.; Parak, W. J.; Nienhaus, G. U. A Quantitative Fluorescence Study of Protein Monolayer Formation on Colloidal Nanoparticles. *Nat. Nanotechnol.* **2009**, *4*, 577–580.
39. Meziani, F.; Tesse, A.; Andriantsitohaina, R. Microparticles Are Vectors of Paradoxical Information in Vascular Cells Including the Endothelium: Role in Health and Diseases. *Pharmacol. Rep.* **2008**, *60*, 75–84.
40. Morel, O.; Toti, F.; Hugel, B.; Freyssinet, J. M. Cellular Microparticles: A Disseminated Storage Pool of Bioactive Vascular Effectors. *Curr. Opin. Hematol.* **2004**, *11*, 156–164.
41. Leroyer, A. S.; Ebrahimian, T. G.; Cochain, C.; Recalde, A.; Blanc-Brude, O.; Mees, B.; Vilar, J.; Tedgui, A.; Levy, B. I.; Chimini, G.; *et al.* Microparticles from Ischemic Muscle Promotes Postnatal Vasculogenesis. *Circulation* **2009**, *119*, 2808–2817.
42. Burnier, L.; Fontana, P.; Kwak, B. R.; Angelillo-Scherrer, A. Cell-Derived Microparticles in Haemostasis and Vascular Medicine. *Thromb. Haemost.* **2009**, *101*, 439–451.
43. Mallat, Z.; Benamer, H.; Hugel, B.; Benessiano, J.; Steg, P. G.; Freyssinet, J. M.; Tedgui, A. Elevated Levels of Shed Membrane Microparticles with Procoagulant Potential in the Peripheral Circulating Blood of Patients with Acute Coronary Syndromes. *Circulation* **2000**, *101*, 841–843.
44. Werner, N.; Wassmann, S.; Ahlers, P.; Kosiol, S.; Nickenig, G. Circulating CD31+/Annexin V+ Apoptotic Microparticles Correlate with Coronary Endothelial Function in Patients with Coronary Artery Disease. *Arterioscler., Thromb., Vasc. Biol.* **2006**, *26*, 112–116.
45. Stabile, E.; Kinnaird, T.; la Sala, A.; Hanson, S. K.; Watkins, C.; Campia, U.; Shou, M.; Zbinden, S.; Fuchs, S.; Kornfeld, H.; *et al.* CD8+ T Lymphocytes Regulate the Arteriogenic Response to Ischemia by Infiltrating the Site of Collateral Vessel Development and Recruiting CD4+ Mononuclear Cells through the Expression of Interleukin-16. *Circulation* **2006**, *113*, 118–124.
46. Furie, B.; Furie, B. C. Cancer-Associated Thrombosis. *Blood Cell. Mol. Dis.* **2006**, *36*, 177–181.
47. Swairjo, M. A.; Concha, N. O.; Kaetzel, M. A.; Dedman, J. R.; Seaton, B. A. Ca(2+)-Bridging Mechanism and Phospholipid Head Group Recognition in the Membrane-Binding Protein Annexin V. *Nat. Struct. Biol.* **1995**, *2*, 968–974.
48. Choksakulnimitr, S.; Masuda, S.; Tokuda, H.; Takakura, Y.; Hashida, M. *In Vitro* Cytotoxicity of Macromolecules in Different Cell Culture Systems. *J. Controlled Release* **1995**, *34*, 9.
49. Baez, S. An Open Cremaster Muscle Preparation for the Study of Blood Vessels by *In Vivo* Microscopy. *Microvasc. Res.* **1973**, *5*, 384–394.
50. Guo, Y.; Lindbom, L.; Hedqvist, P. Spontaneous Leukocyte Rolling in Rat and Mouse Microvessels Is Independent of Mast Cell Activity. *Inflammation Res.* **2000**, *49*, 325–329.
51. Reichel, C. A.; Khandoga, A.; Anders, H. J.; Schlondorff, D.; Luckow, B.; Krombach, F. Chemokine Receptors Ccr1, Ccr2, and Ccr5 Mediate Neutrophil Migration to Postischemic Tissue. *J. Leukocyte Biol.* **2006**, *79*, 114–122.
52. Reichel, C. A.; Rehberg, M.; Lerchenberger, M.; Berberich, N.; Bihari, P.; Khandoga, A. G.; Zahler, S.; Krombach, F. Ccl2 and Ccl3 Mediate Neutrophil Recruitment *via* Induction of Protein Synthesis and Generation of Lipid Mediators. *Arterioscler., Thromb., Vasc. Biol.* **2009**, *29*, 1787–1793.
53. Kubes, P.; Granger, D. N. Leukocyte−Endothelial Cell Interactions Evoked by Mast Cells. *Cardiovasc. Res.* **1996**, *32*, 699–708.
54. Reichel, C. A.; Lerchenberger, M.; Uhl, B.; Rehberg, M.; Berberich, N.; Zahler, S.; Wymann, M. P.; Krombach, F. Plasmin Inhibitors Prevent Leukocyte Accumulation and Remodeling Events in the Postischemic Microvasculature. *PLoS One* **2011**, *6*, e17229.
55. Nomura, S.; Tandon, N. N.; Nakamura, T.; Cone, J.; Fukuhara, S.; Kambayashi, J. High-Shear-Stress-Induced Activation of Platelets and Microparticles Enhances Expression of Cell Adhesion Molecules in THP-1 and Endothelial Cells. *Atherosclerosis* **2001**, *158*, 277–287.
56. Mesri, M.; Altieri, D. C. Leukocyte Microparticles Stimulate Endothelial Cell Cytokine Release and Tissue Factor Induction in a JNK1 Signaling Pathway. *J. Biol. Chem.* **1999**, *274*, 23111–23118.
57. Khandoga, A. G.; Khandoga, A.; Reichel, C. A.; Bihari, P.; Rehberg, M.; Krombach, F. *In Vivo* Imaging and Quantitative Analysis of Leukocyte Directional Migration and Polarization in Inflamed Tissue. *PLoS One* **2009**, *4*, e4693.
58. Nieuwland, R.; Berckmans, R. J.; McGregor, S.; Boing, A. N.; Romijn, F. P.; Westendorp, R. G.; Hack, C. E.; Sturk, A. Cellular Origin and Procoagulant Properties of Microparticles in Meningococcal Sepsis. *Blood* **2000**, *95*, 930–935.